ACS OMEGA

http://pubs.acs.org/journal/acsodf

Article

Superparamagnetic and Perfect-Paramagnetic Zinc Ferrite Quantum Dots from Microwave-Assisted Tunable Synthesis

Kanak Pal S. Parmar, Jeong Hun Kim, Amita Bist, Piyush Dua, Pawan K. Tiwari, Anukorn Phuruangrat, and Jae Sung Lee*

Cite This: *ACS Omega* 2022, 7, 31607−31611

Read Online

ACCESS | Metrics & More | Article Recommendations | Supporting Information

ABSTRACT: The properties of quantum dot (QD)-size material depend directly upon its unit cell structure. Spinel zinc ferrite QD powder is produced via a one-pot microwave-assisted hydrothermal synthesis for just 5 min. Varying initial pH values of the preparation sol from 6 to 12 enlarges the Zn/Fe atomic ratio (by ca. 10%), unit cell volume (by ca. 0.5%), particle size (3.5−4.5 nm), and degree of inversion. This leads to a change in the magnetic behavior of the QD-size zinc ferrite from a superparamagnetic to a perfect-paramagnetic type. This novel finding points that the significant changes in the inherent structural parameters of spinel $ZnFe_2O_4$ QDs (Zn/Fe ratio and degree of inversion) induced by the systematic pH change of the preparation sol are exclusively responsible for the observed unique magnetic behavior instead of mere QD (single domain) nanosizes.

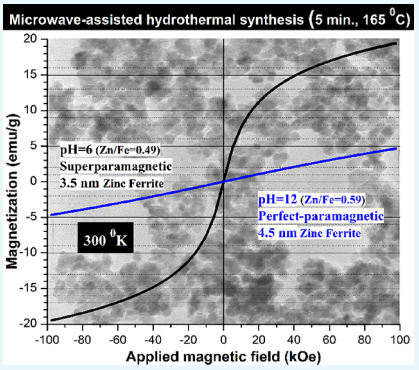

INTRODUCTION

Zinc ferrite ($ZnFe_2O_4$) is used in multiple forms in various fields of photocatalysis, spintronics, sensors, energy and information storage, etc.[1−10] The performance of this material in these applications depends critically upon an interplay of a number of intrinsic (surface/bulk defects, valence, vacancies, Zn/Fe ratio, and inversion parameter) and extrinsic (morphology and size/shape) properties.[2−10] In particular, it is always interesting to prepare a nanosize entity of this face-centered cubic (FCC) material through safe, simple, rapid, and cost-effective synthetic approaches. More importantly, these approaches must be amenable to controlling one or two of the intrinsic variables mentioned above. One preferable synthesis approach with such attributes is direct dielectric heating of a liquid dispersion, known as a microwave-assisted hydrothermal method.[11−13] This method has gained attention not only due to its simplicity and short synthesis time but also because it could bring up reproducible synchronous tailoring of the intrinsic variables quickly via the specific role of synthesis parameters (salt, concentration, solvent, time, temperature, binder, and nature of pH of the adjusting agent).[11−13]

Herein, we report a rapid (ca. 5 min) synthesis of superparamagnetic (SP) cum perfect-paramagnetic (PP) $ZnFe_2O_4$ powder nanomaterial of a quantum dot (QD) size, utilizing a simple sol dispersion whose initial pH (as the single parameter) was precisely controlled using a non-complexing NaOH solution. A number of powder samples were synthesized under a wide range of pH environments (2 to 12), while strictly maintaining all other synthesis parameters to be invariant.

RESULTS AND DISCUSSION

The first direct eye observation was unique and with differentiable colors (e.g., brown and/or tan, etc.) of the individual powder samples, which are clearly noticed in optical photographs in Figure S1. Such differentiated colors of the powder materials could be associated with their distinct inherent properties. Remarkably, using the current recipe of sol dispersion, the impurity-free QD-size $ZnFe_2O_4$ structure was formed only when the initial pH value of the sol dispersion was set above 5 (see XRD patterns of all samples in Figure S2 and structural data in Table S1). Since no binder or additive is used in the synthesis, this unwanted phase formation at a pH of less than 6 is perhaps caused by a solubility difference of metal hydroxo complexes at a specific pH and reaction temperature, which leads to the main byproduct hematite (Fe_2O_3) and other stable oxide impurities.[14−18] Without paying much attention to the detailed mechanism of the phase formation, here, we focus on the comparative room-temperature magnetic properties of spinel $ZnFe_2O_4$ samples with two QD sizes synthesized under mildly acidic (pH = 6) and strongly basic (pH = 12) conditions.

Received: July 24, 2022
Accepted: August 10, 2022
Published: August 23, 2022

Powder X-ray diffraction (XRD) patterns of these $ZnFe_2O_4$ QD samples are displayed in Figure 1. Both samples show broad symmetric XRD patterns with all peaks directly indexed to the face-centered cubic (FCC) $ZnFe_2O_4$ crystal structure (space group $Fd\bar{3}m/227$), indicating that they are single-phase nanocrystalline materials.[4−6,9] However, a unique effect of different pH environments is revealed in a 2θ shift of ca. 0.35° in all XRD peaks, indicating a ca. 0.5% larger lattice constant (L_{FCC}) for the sample synthesized at pH = 12 than that of the sample prepared at pH = 6.[19] The crystallite size and unit cell parameters of synthesized samples were estimated by applying Scherrer's formula on the (311) XRD peak and the equation $L = d_{hkl}(h^2 + k^2 + l^2)^{1/2}$, where d_{hkl} = the interspacing of two nearest hkl planes, which is applicable to a cubic symmetry. The L_{FCC} is calculated by averaging values of all major peaks that appeared in the XRD pattern.

As shown in Table 1, the average crystallite sizes estimated from XRD (3.5 and 4.5 nm for samples prepared at a pH of 6 and 12, respectively) are consistent with the mean particle sizes (3.5 and 4.8 nm, respectively), those obtained from transmission electron microscopy (TEM) images (Figure 2 and Figure S3). A narrow and homogeneous particle size distribution with a minimal significant variation in the spheroid shape is evident in TEM images in both of the pristine samples (Figure S3). The brightness of the selected area electron diffraction (ED) ring pattern in insets of microscopic images and a high-resolution TEM image also support the crystalline nature of the powder samples (Figure S3). The optical band gaps (Figure S4; UV−vis spectra) of powder samples, namely, ca. 2.15 eV (3.5 nm) and ca. 2.19 eV (4.5 nm), are much higher than those typically reported (1.8−2.0 eV) for much larger sizes of $ZnFe_2O_4$ materials.[3,30] All the above results clearly indicate that the pH of the synthesis sol dictates the structural properties of the as-synthesized $ZnFe_2O_4$ QD powder samples.

The high-resolution X-ray photoelectron spectroscopy (XPS) Zn spectra are displayed in Figure 2i (Figure S5 for Fe and O spectra). The binding energy (BE) was calibrated with respect to the reference C 1s peak (284.6 eV) of

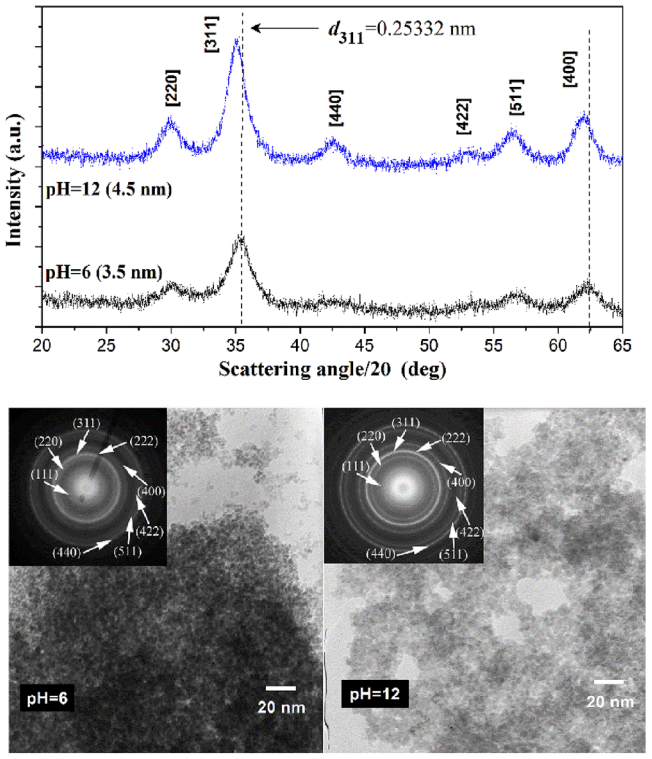

Figure 1. XRD (indexed) patterns and TEM images (insets; indexed diffraction ring patterns) of spinel $ZnFe_2O_4$ QD powder samples as synthesized within 5 min of microwave irradiation at 165−170 °C under different initial pH environments. The curves are vertically offset by a constant factor. The estimated QD sizes (in parentheses) by XRD are also indicated.

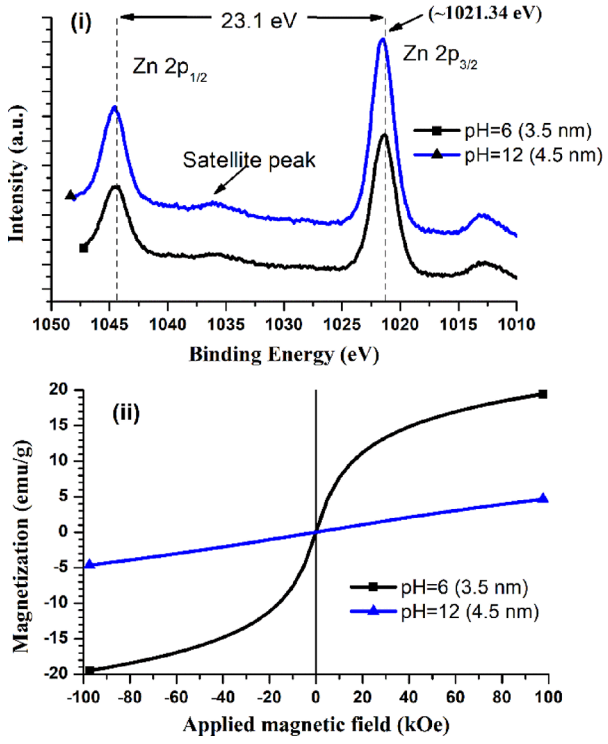

Figure 2. (i) High-resolution XPS spectra of Zn and (ii) superparamagnetic (sigmoidal; Zn/Fe ratio ≈ 0.49) and perfect paramagnetic (linear; Zn/Fe ratio ≈ 0.59) profiles (at 300 °K) of QD-size (parentheses) spinel $ZnFe_2O_4$ samples (numerical data in Table 1).

Table 1. Inherent Properties, Raman Modes [A_{1g} and $F_{2g}(2)$], and Magnetic Data (at 300 K) of Quantum Dot (QD)-Size Spinel $ZnFe_2O_4$ Samples

sample	average crystallite/particle size[a] (nm)	L_{FCC} (V_{FCC}) (Å; Å^3)	binding energy (eV) of Zn (Fe) [O]	element (%) Zn (Fe) [O]	Zn/Fe ratio[b]	Raman (cm^{-1}) A_{1g} [$F_{2g}(2)$]	M_s (H_c)[c] (emu/g, Oe)
pH = 6	3.5 (3.5)	8.41902 (596.7)	1021.34 (711.34) [529.94]	15.1 (15.0) [69.9]	1.006 (0.49)	584 [635]	19.5 (8.9)
pH = 12	4.5 (4.8)	8.45452 (604.3)	1021.46 (711.46) [529.96]	16.9 (15.3) [67.8]	1.101 (0.59)	381 [333]	4.7 (6.7)

[a]By XRD (TEM in parenthesis). V_{FCC} = unit cell volume. [b]By XPS (ICP-MS in parenthesis). [c]M_s (saturation magnetization at 100 kOe) and H_c (coercive force).

https://doi.org/10.1021/acsomega.2c04668
ACS Omega 2022, 7, 31607−31611

adventitious carbon in the sample. The BE analysis of XPS peaks indicated that both samples consisted of Zn^{2+}, Fe^{3+}, and O^{2-} ions, and the BEs of cations are very close to that of a standard FCC spinel zinc ferrite structure (Zn ≈ 1021.40 eV; Zn/Fe ratio = 0.5, degree of inversion = 0).[4,5,9] However, the pH = 12 sample (4.5 nm) has a ca. 10% higher Zn/Fe atomic ratio and ca. 0.12 eV higher BE values for Zn^{2+} and Fe^{3+} cations relative to its counterpart pH = 6 sample (3.5 nm). This extra Zn/Fe ratio is consistent with the result of a ca. 0.5% larger L_{FCC} caused by the larger ionic size of Zn^{2+} (0.74 pm) than that of Fe^{3+} (0.63 pm),[2,19,20] but the Zn/Fe ratios determined by XPS are much larger than the ideal stoichiometry of $ZnFe_2O_4$ (Zn/Fe = 0.5). However, the overall Zn/Fe ratios determined using an inductively coupled plasma mass spectrometry (ICP-MS) technique (Table 1 and Figure S5) are close to the stoichiometry. Still, the ICP-MS results also confirm a ca. 10% higher Zn/Fe atomic ratio for the pH = 12 sample (0.59) than for the pH = 6 sample (0.49), which is consistent with the XPS results. Thus, the unexpectedly high Zn/Fe ratios from the XPS analysis are caused by the surface-sensitive XPS technique and indicate that Zn ions prefer to reside near the surface of QD-size particles.[21−23] This segregation of a particular ion to the surface is known as the self-purification effect, which is common in ultrasmall structures due to their small interior volume.[21−23]

Since the BE of ionic species depends on the bonding strength and surrounding environment, a significant change in the BE indicates that the initial pH of the preparation sol plays a pivotal role that forces some Zn^{2+} and Fe^{3+} to change their occupancy preference between two interlattice subsites (tetrahedral ↔ octahedral) in the synthesized $ZnFe_2O_4$ QD samples. Due to a non-stoichiometric Zn/Fe ratio, the degree of inversion might be greater than 0 in either of the QD-size powder samples.[6,19,20,24,25] This difference in the inversion state is further verified by measuring the static magnetic response. Thus, Figure 2ii shows the room-temperature static magnetization profiles of $ZnFe_2O_4$ QDs, which demonstrates an immense difference in the magnetic behavior of the two QD size samples (Table 1). The 3.5 nm $ZnFe_2O_4$ (nearly stoichiometric Zn/Fe ratio = 0.49 by ICP-MS) reveals a sigmoidal superparamagnetic (SP) profile, whereas the 4.5 nm QD sample (non-stoichiometric Zn/Fe ratio = 0.59 by ICP-MS) shows a linear perfect-paramagnetism (PP) behavior. This observation is surprising as the SP particle (3.5 nm) has a smaller (by ca. 0.5%) unit cell size/volume than that of the PP sample (4.5 nm). Therefore, for comparison purpose, any of the minor magnetic contributions (coercivity, magnetization, and magnetic profile) arising from extrinsic variables (size, shape, surface area, volume, and rotation of a single domain; domain boundary effects; and canting and anisotropy of surfaces) and intrinsic unit cell factors (crystallinity, directional order, and L_{FCC} or V_{FCC}) could be safely neglected at first sight in both spinel $ZnFe_2O_4$ QD samples.[10,19,20,24−26]

A striking difference in the relative degree of inversion between the two pristine $ZnFe_2O_4$ QD powder samples is clearly visible in the high-resolution A_{1g} and $Fe_{2g}(2)$ Raman modes in Figure 3 (data in Table 1). The lower (584 cm^{-1}) and higher (635 cm^{-1}) wavenumber positions of the A_{1g} peak (tetrahedral group) in 3.5 and 4.5 nm-size samples resemble higher and lower numbers of tetrahedron ZnO_4 units, respectively, thus reflecting a lesser inversion state in the 3.5 nm $ZnFe_2O_4$ (synthesized at pH = 6) sample than that of 4.5 nm $ZnFe_2O_4$ (synthesized at pH = 12).[6,27−30] Also, the $F_{2g}(2)$ (octahedral group) peak position of the 3.5 nm sample (381.6 cm^{-1}) is higher than that of the 4.5 nm sample (333.2 cm^{-1}); therefore, this higher side shift is cognate with the lower number of octahedron FeO_6 units, which again indicates a lesser inversion parameter of the 3.5 nm sample than that of the 4.5 nm sample.[27−30]

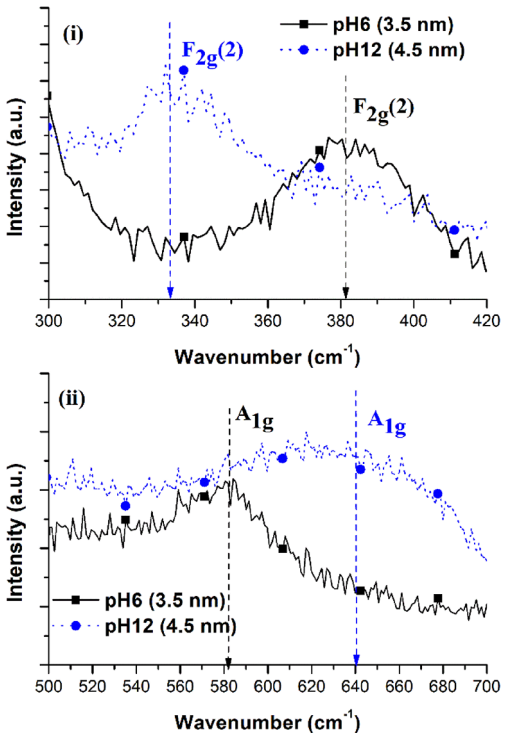

Figure 3. High-resolution Raman spectra of superparamagnetic (3.5 nm; pH = 6) and perfect-paramagnetic (4.5 nm; pH = 12) spinel $ZnFe_2O_4$ QD samples (see Figure S6 and Table S2 for all Raman active modes).

Figure S7i shows the temperature-dependent magnetic profiles of almost identical QD-sized particles where a clear drastic difference is easily observed between the magnetization behavior and thermal fluctuations of particles. The absence of particle interactions (negligible coercivity) suggests that the dissimilar structural parameters (Zn/Fe ratio, inversion state, and lattice parameter) together with uncompensated surface spins (paramagnetic type) of QD-size particles ultimately control the magnetization of powder samples.[8,19,31−33] As a result, at a constant low temperature (e.g., 50 °K; Figure S7ii), the effect of the dissimilar core (data in Table 1 and Table S3) becomes more pronounced in a near-zero applied magnetic field, and a sharp ferrimagnetism (FiM) response is observed in a nearly stoichiometric (3.5 nm) sample as opposed to an extremely poor FiM in a Zn-enriched (4.5 nm) sample. The higher inversion and excessive nonmagnetic Zn causes a magnetic frustration (disorder) in a non-stoichiometric (4.5 nm) sample by disrupting the magnetic coupling of lattice-site interactions that eventually leads to perfect paramagnetism at room temperature.[19] Hence, the analyses (XRD, XPS, ICP-MS, TEM, and Raman) consistently confirm that the single sol parameter (pH) is sufficient to control the inherent structural parameters (phase purity, particle size, and its narrow size distribution, Zn/Fe ratio, L_{FCC}, and degree of inversion) of the spinel-type $ZnFe_2O_4$ nanomaterial.

https://doi.org/10.1021/acsomega.2c04668
ACS Omega 2022, 7, 31607−31611

Additionally, the degree of inversion in this powder material is accompanied by the unique SP and/or PP evolution. To further confirm this, an inversion was boosted in the SP $ZnFe_2O_4$ sample (3.5 nm) by heating it at an elevated temperature (3 °C/min, 460 °C, 1 h, air) inside a laboratory furnace.[29] As shown in Figure S8 (data in Table S3), although this heating promoted better crystallinity and formed a larger particle (3.5−7.2 nm), it also drastically reduced the SP profile and the saturation magnetization (19.5 to 9.1 emu/g), which is expected owing to its relatively higher degree of inversion rather than its bigger QD size (characteristic length scale). This result also leads to the conclusion in that one intrinsic unit cell parameter (Zn/Fe ratio and/or a resulted degree of inversion) of each pristine QD size particle (3.5 or 4.5 nm) is exclusively responsible for the unique magnetic behavior (SP and/or PP) of spinel $ZnFe_2O_4$ QDs, not merely their nanosizes.

CONCLUSIONS

In summary, for the first time, to the best of our knowledge, a dual magnetic behavior (superparamagnetism and/or perfect paramagnetism) is observed in a QD-size spinel $ZnFe_2O_4$ nanomaterials, which is synthesized via a rapid (5 min) and facile microwave-assisted hydrothermal synthesis process under varying pH values of the preparation sol. It is interesting that the flipped magnetism is achieved by simply varying the initial pH of the sol dispersion, which modifies the Zn/Fe ratio and inversion parameter of the QD-size $ZnFe_2O_4$ powder. Thus, the observed drastic transition of the unique magnetic behavior and the magnetic properties is due to significant changes in the intrinsic structural parameters of spinel $ZnFe_2O_4$ (Zn/Fe ratio and inversion parameter), instead of merely QD (single domain) sizes.

EXPERIMENTAL SECTION

As-purchased reagent-grade chemicals (Samchun Chemical Co., Korea) were used. To prepare the $ZnFe_2O_4$ QD powder nanomaterial, a simple sol dispersion was made by mixing appropriate amounts of Zn/Fe nitrate hexahydrates (1−2 mole ratio) in a 60 mL triple-deionized water (Millipore, resistivity of ∼18 $M\Omega^{-1}$) while closely controlling its pH by dropwise addition of a non-complexing NaOH solution under constant mild magnetic stirring (ca. 20 min). The sol was then kept inside a sealed digestive Teflon vessel (ca. 100 mL) for only 5 min at 165−170 °C (ramp of 10 °C/min.) under microwave irradiation (MDS-2000, 2.45 GHz, 1200 W, CEM Corporation, USA). The vessel was cooled naturally, and the powder samples (weight yield of ca. 85%) were obtained after excessively (three times) washing the filtrates with distilled water and then overnight vacuum drying in a laboratory oven.

The optical images of powder samples were captured using an ordinary digital camera (Sony). The phase, particle, structural composition, optical band-gap characteristics, and magnetic profiles/properties of samples were determined using X-ray diffraction (XRD, Cu Kα, PRO-MPD, Philips), transmission electron microscopy (TEM, Cs-corrected JOEL, JEM-2200FS), X-ray photoemission spectroscopy (XPS, HR-XPS; VG Scientific ESCA LAB 220-IXL), ICP-MS system (Agilent, USA), Raman (alpha300R WITec, excitation of ∼532 nm), diffuse reflectance spectra (300−800 nm, integrated sphere method, Shimadzu), a vibrating sample magnetometer (VSM, Lake Shore), and Quantum Design PPMS VersaLab.

ASSOCIATED CONTENT

Supporting Information

The Supporting Information is available free of charge at https://pubs.acs.org/doi/10.1021/acsomega.2c04668.

Optical photographs of all synthesized samples; XRD patterns, estimated crystallite or particle sizes, and unit cell parameters of all $ZnFe_2O_4$ samples; bright-field TEM images and electron diffraction ring patterns of pristine QD $ZnFe_2O_4$ samples (3.5 nm, pH = 6; 4.5 nm, pH = 12); high-resolution TEM image (red-line fringe spacing of ∼0.26 nm; 311 exposed surface) and particle size distribution (histograms) of zinc ferrite powder samples; UV−vis diffuse reflectance spectra and Tauc plots of pristine QD $ZnFe_2O_4$ samples; high-resolution XPS spectra (Zn, Fe, and O) of pristine QD $ZnFe_2O_4$ samples; ICP-MS results; room temperature (300 °K) and low temperature (50−200 °K) magnetic profiles of pristine and heat-treated (460 °C, 1 h, air) $ZnFe_2O_4$ samples; room-temperature full Raman spectra and positions of all five active Raman modes (A + E+3F) of pristine QD $ZnFe_2O_4$ samples; and Raman spectra of the heat-treated pristine QD $ZnFe_2O_4$ sample (PDF)

AUTHOR INFORMATION

Corresponding Author

Jae Sung Lee − *School of Energy and Chemical Engineering, Ulsan National Institute of Science and Technology (UNIST), Ulsan 44919, South Korea;* orcid.org/0000-0001-6432-9073; Email: jlee1234@unist.ac.kr

Authors

Kanak Pal S. Parmar − *Department of Physics, University of Petroleum and Energy Studies (UPES), Dehradun 248007, India*

Jeong Hun Kim − *School of Energy and Chemical Engineering, Ulsan National Institute of Science and Technology (UNIST), Ulsan 44919, South Korea*

Amita Bist − *Department of Science, Atal Utkrisht Government Inter College, Uttarkashi 249193, India*

Piyush Dua − *College of Applied Sciences, Suhar University of Technology and Applied Sciences, Muscat 133, Oman;* orcid.org/0000-0002-5444-1384

Pawan K. Tiwari − *Department of Physics, Birla Institute of Technology, Ranchi 835215, India;* orcid.org/0000-0003-0239-2071

Anukorn Phuruangrat − *Division of Physical Science, Faculty of Science, Prince of Songkla University, Songkhla 90110, Thailand*

Complete contact information is available at: https://pubs.acs.org/10.1021/acsomega.2c04668

Notes

The authors declare no competing financial interest.

ACKNOWLEDGMENTS

This work was supported by the Climate Change Response Project (no. NRF-2019M1A2A2065 612) and Brainlink Project (no. NRF-2022H1D3A3A01081140) funded by the Ministry of Science and ICT of Korea via the National Research Foundation and by research funds from Hanhwa Solutions Chemicals and UNIST (no. 1.190013.01).

REFERENCES

(1) Goldman, A. *Modern Ferrite Technology*; 2nd ed., Springer, 2006.
(2) Yang, Y.; Liu, X.; Yang, Y.; Xiao, W.; Li, Z.; Xue, D.; Li, F.; Ding, J. Synthesis of nonstoichiometric zinc ferrite nanoparticles with extraordinary room temperature magnetism and their diverse applications. *J. Mater. Chem. C* **2013**, *1*, 2875−2885.
(3) Kim, J. H.; Kim, H. E.; Kim, J. H.; Lee, J. S. Ferrites: Emerging light absorbers for solar water splitting. *J. Mater. Chem. A* **2020**, *8*, 9447−9482.
(4) Ma, J.; Xiong, Y.; Dai, X.; Yu, F. Zinc Spinel ferrite nanoparticles as a pseudocapacitive electrode with ultrahigh desalination capacity and long-term stability. *Environ. Sci. Technol. Lett.* **2020**, *7*, 118−125.
(5) Harada, M.; Kuwa, M.; Sato, R.; Teranishi, T.; Takahashi, M.; Maenosono, S. Cation Distribution in monodispersed MFe_2O_4 (M = Mn, Fe, Co, Ni, and Zn) nanoparticles investigated by X-ray absorption fine structure spectroscopy: Implications for magnetic data storage, catalysts, sensors, and ferrofluids. *ACS Appl. Nano Mater.* **2020**, *3*, 8389−8402.
(6) Blanco-Gutiárrez, V.; Andrada-Chacón, A.; Sánchez-Benítez, J.; Urones-Garrote, E.; Sáez-Puche, R.; Torralvo-Fernández, M. J. Superparamagnetic behavior at room temperature through crystal chemistry modification and particle assembly formation: Zinc and nickel ferrite systems. *J. Phys. Chem. C* **2019**, *123*, 16973−16981.
(7) Kolhatkar, A.; Jamison, A.; Litvinov, D.; Willson, R.; Lee, T. Tuning the magnetic properties of nanoparticles. *Int. J. Mol. Sci.* **2013**, *14*, 15977−16009.
(8) Hochepied, J. F.; Bonville, P.; Pileni, M. P. Nonstoichiometric zinc ferrite nanocrystals: Syntheses and unusual magnetic properties. *J. Phys. Chem. B* **2000**, *104*, 905−912.
(9) Zhang, Y.; Shi, Q.; Schliesser, J.; Woodfield, B. F.; Nan, Z. Magnetic and thermodynamic properties of nanosized Zn ferrite with normal spinal structure synthesized using a facile method. *Inorg. Chem.* **2014**, *53*, 10463−10470.
(10) Binns, C. Nanomagnetism: Fundamentals and Applications. *Front. Nanosci.* **2014**, *6*, 1−31.
(11) Bilecka, I.; Niederberger, M. Microwave chemistry for inorganic nanomaterials synthesis. *Nanoscale* **2010**, *2*, 1358.
(12) Phuruangrat, A.; Kuntalue, B.; Dumrongrojthanath, P.; Thongtem, T.; Thongtem, S. Microwave-assisted solvothermal synthesis of cubic ferrite (MFe_2O_4, M = Mn, Zn, Cu and Ni) nanocrystals and their magnetic properties. *Dig. J. Nanomater. Biostruct.* **2018**, *13*, 563−568.
(13) Parmar, K. P. S.; Ramasamy, E.; Lee, J.; Lee, J. S. Rapid (∼10 min) synthesis of single-crystalline, nanorice TiO_2 mesoparticles with a high photovoltaic efficiency of above 8%. *Chem. Commun.* **2011**, *47*, 8572−8574.
(14) Pourbaix, M. *Atlas of electrochemical equilibria in - aqueous solutions*; National Association of Corrosion Engineers: Houston, Texas, USA, 1974.
(15) Rose, A. L.; Bligh, M. W.; Collins, R. N.; Waite, T. D. Resolving early stages of homogeneous Iron (III) oxyhydroxide formation from Iron (III) nitrate solutions at pH 3 using time-resolved SAXS. *Langmuir* **2014**, *30*, 3548−3556.
(16) Pham, A. N.; Rose, A. L.; Feitz, A. J.; Waite, T. D. Kinetics of Fe(III) precipitation in aqueous solutions at pH 6.0−9.5 and 25 °C. *Geochim. Cosmochim. Acta* **2006**, *70*, 640−650.
(17) Toshio, T.; Masao, K.; Hideo, T.; Toshihiro, A.; Mikio, T.; Norihiko, N. Effect of pH values on the formation and solubility of zinc compounds. *Bull. Inst. Chem. Res.* **1978**, *56*, 242−246.
(18) Beverskog, B.; Puigdomenech, I. Revised pourbaix diagrams for zinc at 25-300 °C. *Corros. Sci.* **1997**, *39*, 107−114.
(19) Cobos, M. A.; de la Presa, P.; Llorente, I.; Alonso, J. M.; García-Escorial, A.; Marín, P.; Hernando, A.; Jiménez, J. A. Magnetic phase diagram of nanostructured zinc ferrite as a function of inversion degree *δ*. *J. Phys. Chem. C* **2019**, *123*, 17472−17482.
(20) Zamiri, R.; Salehizadeh, S. A.; Ahangar, H. A.; Shabani, M.; Rebelo, A.; Kumar, J. S.; Soares, M. J.; Valente, M. A.; Ferreir, J. M. F. Optical and magnetic properties of $ZnO/ZnFe_2O_4$ nanocomposite. *NANO* **2017**, *192*, 330−338.
(21) Dalpian, G. M.; Chelikowsky, J. R. Self-purification in semiconductor nanocrystals. *Phys. Rev. Lett.* **2006**, *96*, No. 226802.
(22) Anitha, M.; Khadar, M. A.; Banerjee, A. Paramagnetic behavior of Co doped TiO_2 nanocrystals controlled by self-purification mechanism. *J. Solid State Chem.* **2016**, *239*, 237−245.
(23) Kovalenko, M. V.; Manna, L.; Cabot, A.; Hens, Z.; Talapin, D. V.; Kagan, C. R.; Klimov, V. I.; Rogach, A. L.; Reiss, P.; Milliron, D. J.; et al. Prospects of Nanoscience with Nanocrystals. *ACS Nano* **2015**, *9*, 1012−1057.
(24) Thirupathi, G.; Singh, R. Magnetic properties of zinc ferrite nanoparticles. *IEEE Trans. Magn.* **2012**, *48*, 3630−3633.
(25) John, S. P.; Mathew, J. Determination of ferromagnetic, superparamagnetic and paramagnetic components of magnetization and the effect of magnesium substitution on structural, magnetic and hyperfine properties of zinc ferrite nanoparticles. *J. Magn. Magn. Mater.* **2019**, *475*, 160−170.
(26) Yokoyama, M.; Ohta, E.; Sato, T.; Komaba, T.; Sato, T. Size dependent magnetic properties of zinc ferrite fine particles. *J. Phys. IV* **1997**, *07*, 521−522.
(27) Nikolic, M. V.; Vasiljevic, Z. Z.; Lukovic, M. D.; Pavlovic, V. P.; Krstic, J. B.; Vujancevic, J.; Tadic, N.; Vlahovic, B.; Palovic, V. B. Investigation of $ZnFe_2O_4$ spinel ferrite nanocrystalline screen-printed thick films for application in humidity sensing. *Int. J. Appl. Ceram. Technol.* **2019**, *16*, 981−993.
(28) Granone, L. I.; Ulpe, A. C.; Robben, L.; Klimke, S.; Jahns, M.; Renz, F.; Gesing, T. M.; Bredow, T.; Dillert, R.; Bahnemann, D. W. Effect of the degree of inversion on optical properties of spinel $ZnFe_2O_4$. *Phys. Chem. Chem. Phys.* **2018**, *20*, 28267−28278.
(29) Rivero, M.; Campo, A. D.; Mayoral, A.; Mazario, E.; Sánchez-Marcos, J.; Muñoz-Bonilla, A. Synthesis and structural characterization of $Zn_xFe_{3-x}O_4$ ferrite nanoparticles obtained by an electrochemical method. *RSC Adv.* **2016**, *6*, 40067−40076.
(30) Ulpe, A. C.; Bauerfeind, K. C.; Granone, B. L. I.; Arsou, A.; Megatif, L.; Dillert, R.; Warfsmann, S.; Taffa, D. H.; Wark, M.; Bahnemann, D. W.; Bredow, T. Photoelectrochemistry of Ferrites: Theoretical Predictions vs. Experimental Results. *Z. Phys. Chem.* **2020**, *234*, 719−776.
(31) Ramon Ramón, J. A.; Ortiz-Quiñonez, J. L.; Ray, A.; Das, S.; Pal, U. Inducing Superparamagnetism and High Magnetization in Nickel Cobaltite ($Ni_xCo_{3-x}O_4$) Spinel Nanoparticles by Controlling Ni mol Fraction and Cation distribution. *J. Phys. Chem. C* **2020**, *124*, 18264−18274.
(32) Atif, M.; Hasanain, S. K.; Nadeem, M. Magnetization of sol−gel prepared zinc ferrite nanoparticles: Effects of inversion and particle size. *Solid State Commun.* **2006**, *138*, 416−421.
(33) Ortiz-Quiñonez, J. L.; Ramón, J. A.; de Anda Reyes, M. E.; Ray, A.; Das, S.; Pal, U. Structure and magnetic behavior of sol-gel grown spinel $Ni_xMn_{3-x}O_4$ nanoparticles: Effect of Ni fraction and induction of superparamagnetism at room temperature. *Mater. Res. Bull.* **2021**, *139*, No. 111267.

https://doi.org/10.1021/acsomega.2c04668
ACS Omega 2022, 7, 31607−31611